Flexural vibration band gaps in Euler-Bernoulli beams with locally resonant structures with two degrees of freedom

Dianlong Yu,* Yaozong Liu, Honggang Zhao, Gang Wang, and Jing Qiu
Institute of Mechatronical Engineering, National University of Defense Technology, Changsha 410073, China
and PBG Research Center, National University of Defense Technology, Changsha 410073, China
(Received 2 November 2005; revised manuscript received 6 December 2005; published 10 February 2006)

Using the transfer matrix theory, we provided the band structure of flexural waves in an Euler-Bernoulli beam with locally resonant structures, with two degrees of freedom, i.e., a resonator with vertical and rotational vibration. The frequency response function of a finite periodic system was calculated by the finite element method. The material damping of rubber makes the gaps wider in the calculation. These theoretical results show a good agreement with those of the experiment. The measured result provides an attenuation of over 20 dB in the frequency range of the band gaps. The existence of low-frequency band gaps in such a beam provides a method of flexural vibration control of beams.

DOI: 10.1103/PhysRevB.73.064301 PACS number(s): 63.20.−e, 43.40.+s, 46.40.Cd

I. INTRODUCTION

In the last decade, the propagation of elastic or acoustic waves in periodic composite materials that are called phononic crystals (PCs) has received much attention.[1–13] In the frequency ranges of complete elastic band gaps, sound and vibration are both forbidden. This is of interest for applications such as frequency filters, vibrationless environments for high-precision mechanical systems, design of new transducers, and so on.

Elastic or acoustic wave band gaps from the Bragg reflection mechanism in periodic beams were researched early.[2–5] In Ref. 2, the authors studied the flexural vibration propagation in straight beams with periodic structures theoretically and experimentally. The periodic beams comprise continuous elements of two different material and geometrical types connected in alternating sequence. Also the Bragg gaps of acoustic waves in waveguides with periodic side branches have been studied theoretically and experimentally.[3–5] The emphasis of these studies[3–5] was on the propagation of the fluid or acoustic wave in a tube with side branches. However, for the Bragg gaps, the spatial modulation must be of the same order as the wavelength in the gap. This would require structures with the size of outdoor sculptures in order to prevent environmental noise or bigger for the vibration shielding of common machines.[1]

The pioneering work of Liu *et al.*[1] opened an additional field of PCs. The authors studied three-dimensional PCs consisting of cubic arrays of coated lead spheres (the coating is a thin film of a soft material) immersed in an epoxy matrix, i.e., locally resonant (LR) PCs. They predicted the appearance of a gap in a frequency range two orders of magnitude lower than the one resulting from Bragg scattering, which spurred further research.[8–10] The two-dimensional counterparts, i.e., lattices of coated cylinders in epoxy, have also been studied.[11–13]

A flexural beam carrying one or several elastically mounted concentrated masses, such as engines, motors, oscillators, or vibration absorbers, is often encountered in the fields of mechanical, civil, and aeronautical engineering.[14,15] An Euler-Bernoulli beam carrying multiple spring-mass systems with one or two degrees of freedom (1DOF or 2DOF) has been researched, but only the natural frequencies of such a constrained Euler-Bernoulli beam system have been considered.[14] The lumped-mass method was introduced to study the band gaps of flexural elastic waves in an infinite beam with LR structures,[6] but the numerical calculation methods are so complex that the authors had to distinguish which dispersive curves are useful for research in flexural waves. The important dispersive curve in the gap for the 2DOF systems was not found.

In this paper, we research flexural vibration band gaps in an Euler-Bernoulli beam with 2DOF LR structures. The band structures of flexural waves in the Euler-Bernoulli beam are calculated with the exact transfer matrix (TM) theory. To compare the band gap of the infinite system and the transmission coefficient of the finite system, the transmission frequency response function (FRF) of a finite sample of the structure is calculated with the finite element (FE) method. Finally all the theoretical results are validated with a vibration experiment.

II. THEORY OF THE TM

Figure 1 shows a simple model of an Euler-Bernoulli beam with periodical 2DOF LR structures. The beam is attached periodically with harmonic oscillators. One LR oscillator consists of two springs k and one mass m. The lattice constant is a.

The governing differential equation for free flexural vibration of the Euler-Bernoulli beam can be written as follows:[17]

$$\frac{\partial^2}{\partial x^2}\left[EI\frac{\partial^2 y(x,t)}{\partial x^2}\right]+\rho A\frac{\partial^4 y(x,t)}{\partial t^4}=0 \tag{1}$$

where ρ and E are the density and Young's modulus, respectively, A is the cross-section area, and I is the moment of inertia with respect to the axis perpendicular to the beam axis. $y(x,t)$ is the dynamic displacement at x. We consider the normal-mode condition $y(x,t)=X(x)\exp(i\omega t)$, where ω is the circular natural frequency.

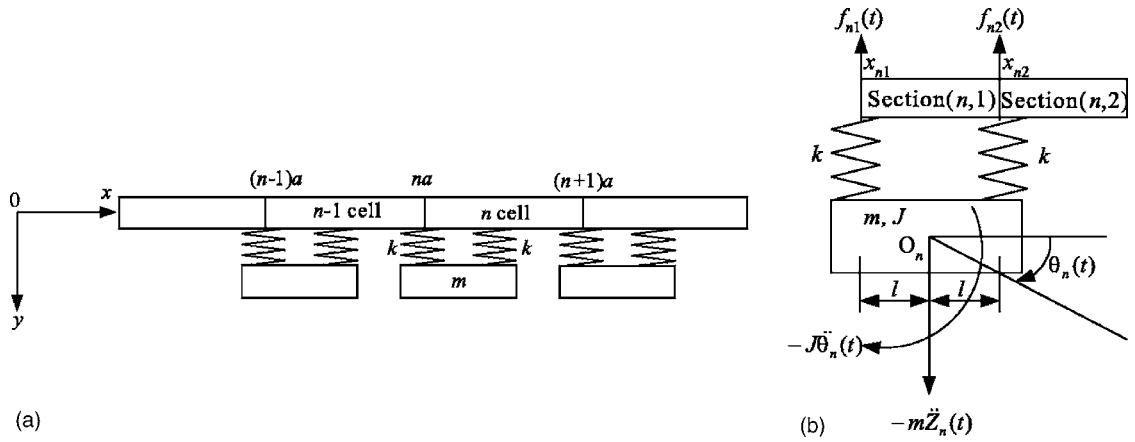

FIG. 1. (a) A simple model of the Euler beam carrying multiple 2DOF LR structures; (b) the force equilibrium of the nth 2DOF LR structure.

For an Euler-Bernoulli beam, the amplitude $X(x)$ reads as

$$X(x) = A\cos(\lambda x) + B\sin(\lambda x) + C\cosh(\lambda x) + D\sinh(\lambda x) \tag{2}$$

where $\lambda^4 = \rho A\omega^2/EI$.

For the first section of the nth cell shown in Fig. 1(b), the amplitude

$$X_{n1}(x') = A_{n1}\cos(\lambda x') + B_{n1}\sin(\lambda x') + C_{n1}\cosh(\lambda x') + D_{n1}\sinh(\lambda x') \tag{3}$$

where $x' = x - na$, $na \leqslant x \leqslant na + l$. Similarly, for the second section of the nth cell, the amplitude can be written

$$X_{n2}(x'') = A_{n2}\cos(\lambda x'') + B_{n2}\sin(\lambda x'') + C_{n2}\cosh(\lambda x'') + D_{n2}\sinh(\lambda x'') \tag{4}$$

where $x'' = x - na$, $na + l \leqslant x \leqslant (n+1)a$.

As for the nth 2DOF LR oscillator, considering the equilibrium condition for all the forces in the y axis, including the inertial force and the moment about the center of the gravity O_n, one obtains[14]

$$-f_{n1}(t) - f_{n2}(t) - m\ddot{Z}_n(t) = 0, \tag{5}$$

$$f_{n1}(t)(O_n - x_{n1}) - J\ddot{\theta}(t) - f_{n2}(t)(x_{n2} - O_n) = 0 \tag{6}$$

where $f_{n1}(t), f_{n2}(t)$ are the interactive forces between the 2DOF LR oscillator and the beam at the two attaching points x_{n1} and x_{n2}, respectively, and m and J are the mass and mass moment of inertia of the oscillator, respectively. $Z_n(t) = V_n\exp(i\omega t)$ is the displacement of the nth LR oscillator at the center of gravity, V_n is the amplitude of displacement. $\theta_n(t) = \alpha_n\exp(i\omega t)$ is the torsional displacement of the nth LR oscillator, and α_n is the rotational angle.

The forces $f_{n1}(t)$ and $f_{n2}(t)$ are given by

$$\begin{aligned} f_{n1}(t) &= k[Z_n(t) - y(x_{n1},t) - (O_n - x_{n1})\theta_n(t)] \\ &= k[V_n - X_{n1}(x_{n1}) - l\alpha_n]\exp(i\omega t) \\ &\triangleq F_{n1}\exp(i\omega t), \end{aligned} \tag{7}$$

$$\begin{aligned} f_{n2}(t) &= k[Z_n(t) - y(x_{n2},t) + (x_{n2} - O_n)\theta_n(t)] \\ &= k[V_n - X_{n2}(x_{n2}) + l\alpha_n]\exp(i\omega t) \\ &\triangleq F_{n2}\exp(i\omega t). \end{aligned} \tag{8}$$

Substituting Eqs. (7) and (8) into Eqs. (5) and (6) leads to

$$V_n = k\frac{X_{n1}(x_{n1}) + X_{n2}(x_{n2})}{2k - m\omega^2}, \tag{9}$$

$$\alpha_n = kl\frac{X_{n1}(x_{n1}) - X_{n2}(x_{n2})}{J\omega^2 - 2kl^2}, \tag{10}$$

where $2l$ is the distance between the two attachment points x_{n1} and x_{n2}.

Using Eqs. (3) and (4), one can obtain

$$X_{n1}(x_{n1}) = X_{n1}(0) = A_{n1} + C_{n1}, \tag{11}$$

$$X_{n2}(x_{n2}) = X_{n2}(l) = A_{n2}\cos(\lambda l) + B_{n2}\sin(\lambda l) + C_{n2}\cosh(\lambda l) + D_{n2}\sinh(\lambda l). \tag{12}$$

These results are now used to deal with the dispersive relation of the Euler-Bernoulli beam with LR structures.

The continuities of displacement, slope, bending moment, and shear force at the attachment points x_{n2}, i.e., $x = na + l$, give

$$X_{n1}(l) = X_{n2}(l), \tag{13a}$$

$$X'_{n1}(l) = X'_{n2}(l), \tag{13b}$$

$$EIX''_{n1}(l) = EIX''_{n2}(l), \tag{13c}$$

$$EIX'''_{n1}(l) = EIX'''_{n2}(l) - F_{n2}. \tag{13d}$$

Substituting Eqs. (3) and (4) into Eqs. (13) and using Eqs. (7) and (8), one can obtain the matrix form

$$\mathbf{K}_1\boldsymbol{\Psi}_{n2} = \mathbf{H}_1\boldsymbol{\Psi}_{n1} \tag{14}$$

where $\boldsymbol{\Psi}_{n2} = [A_{n2}\ B_{n2}\ C_{n2}\ D_{n2}]^T$, $\boldsymbol{\Psi}_{n1} = [A_{n1}\ B_{n1}\ C_{n1}\ D_{n1}]^T$.

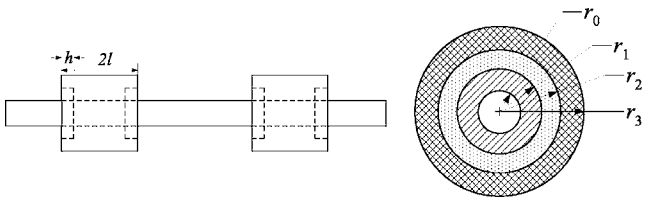

FIG. 2. Model of the Euler-Bernoulli beam with 2DOF LR structures.

The continuities at the attachment points x_{n1}, i.e., $x=na$, give

$$X_{(n-1)2}(a) = X_{n1}(0), \tag{15a}$$

$$X'_{(n-1)2}(a) = X'_{n1}(0), \tag{15b}$$

$$EIX''_{(n-1)2}(a) = EIX''_{n1}(0), \tag{15c}$$

$$EIX'''_{(n-1)2}(a) = EIX'''_{n1}(0) - F_{n1}. \tag{15d}$$

Analogously, one can obtain

$$\mathbf{K}_2\mathbf{\Psi}_{n1} + \mathbf{K}_3\mathbf{\Psi}_{n2} = \mathbf{H}_2\mathbf{\Psi}_{(n-1)2}. \tag{16}$$

Based on Eqs. (14) and (16), the relation between the nth cell and $(n-1)$th cell is given by

$$\mathbf{\Psi}_{n2} = \mathbf{T}\mathbf{\Psi}_{(n-1)2} \tag{17}$$

where $\mathbf{T}=\mathbf{K}_1^{-1}\mathbf{H}_1[\mathbf{K}_2+\mathbf{K}_3\mathbf{K}_1^{-1}\mathbf{H}_1]^{-1}\mathbf{H}_2$ is the transfer matrix.

However, due to the periodicity of the infinite structure in the x direction, the Bloch theorem[18] guarantees

$$\mathbf{\Psi}_{n2} = e^{iqa}\mathbf{\Psi}_{(n-1)2} \tag{18}$$

where q is the wave vector in the x direction.

Inserting Eq. (18) into Eq. (17) yields a standard eigenvalue problem of 4×4 matrix:

$$|\mathbf{T} - e^{iqa}\mathbf{I}| = 0, \tag{19}$$

where $\mathbf{I}$ is the 4×4 unit matrix. In other words, for given ω, Eq. (19) gives the values of q. Depending on whether q is real or has an imaginary part, the corresponding wave propagates through the Euler-Bernoulli beam (passband) or is damped (band gap).

As for a finite sample, attenuation modes in the band gaps can exist. Thus, the propagation of elastic waves within the specific frequency ranges can only be weakened, not totally forbidden. In order to describe the propagation of flexural waves in the finite sample correctly, we employ the FE technique to calculate its transmission FRF.

III. THEORETICAL AND EXPERIMENTAL RESULTS

We design the beam with periodic LR structures shown in Fig. 2. The beam is constructed from an aluminum tube with the inner and outer radii being $r_0=7\times10^{-3}$ and $r_1=1\times10^{-2}$ m, respectively. The unit of the LR structure is composed of a soft rubber ring with outer radius $r_2=1.5\times10^{-2}$ m and a heavy metal Cu ring with outer radius $r_3=1.95\times10^{-2}$ m. The length of the rubber ring is $h=1\times10^{-2}$ m, and the length of the Cu ring is $2l=6\times10^{-2}$ m. The cross-section area of the beam is $A=1.602\times10^{-4}$ m^2 and the moment of inertia $I=5.968\times10^{-9}$ m^4. The lattice constant is $a=1.5\times10^{-1}$ m. ρ_1, E_1, and G_1 are the density, Young's modulus, and shear modulus of rubber; ρ_2 is the density of Cu.

For the rubber ring, the radial stiffness is[19]

$$k = \frac{\pi(5+3.29H^2)G_1h}{\ln(r_2/r_1)} \tag{20}$$

where $H=h/(r_1+r_2)\ln(r_1/r_2)$ is the shape coefficient.

The elastic parameters employed in the calculations are $\rho_{\mathrm{Al}}=2600$ kg/m^3, $E_{\mathrm{Al}}=7.0\times10^{10}$ Pa, $G_{\mathrm{Al}}=2.7\times10^{10}$ Pa, $\rho_{\mathrm{rubber}}=1300$ kg/m^3, $E_{\mathrm{rubber}}=7.7\times10^{6}$ Pa, $G_{\mathrm{rubber}}=2.6\times10^{5}$ Pa, $\rho_{\mathrm{Cu}}=8950$ kg/m^3. Based on Eq. (20), the spring stiffness of the rubber ring is $k=1.65\times10^{5}$ N/m. The mass of the Cu ring is $m=2.6\times10^{-1}$ kg.

Figure 3(a) illustrates the band structure of the Euler-Bernoulli beam with LR structures shown in Fig. 2. We can find one complete band gap within 800 Hz. The low frequency gap extends from a frequency of 176.3 up to 408.8 Hz. The flexural wave cannot propagate through the Euler-Bernoulli beam in this frequency range.

A remarkable feature in Fig. 3(a) is the flat branches crossing the whole Brillouin zone. The branches are real and converged. In order to investigate the reason for the flat bands, we calculate the FRF of the flexural vibration with nine LR oscillators by the FE method. The FRF of vibration has been used to describe the gaps effectively.[16] In the calculation, a white noise in the y direction from 0 to 800 Hz is excited in one end of the beam. The frequency response of the other end of the beam is shown as the continuous line in Fig. 3(b). There is one sharp drop in the frequency response curve extending from 180 to 410 Hz, which is in very good agreement with the band structure. One resonant peak appears in the gap at about 220 Hz, whose frequency corresponds to the second flat band in the band structure. These resonant modes at the selected points T_1, T_2, and T_3 in Fig. 3 are illustrated in Figs. 4(a)–4(c). In Fig. 4, the dashed lines illustrate the primal deformation, and the solid lines illustrate the maximum deformation in vibration. For the point T_1 [Fig. 4(a)], the amplitude of the vibrations is well concentrated in the resonators, and it is very small in the hosting beam. The vibration direction of the resonators is vertical to the beam. At point T_3 [Fig. 4(c)], the lattice vibrations are almost the same except that the vibrations in the hosting beam are notable and in the reverse phase to the resonators. The time-harmonic forces from oscillator to host beam split the original dispersion curves, and a band gap is generated. The rule used to judge whether a resonant mode in PCs can result in a corresponding subfrequency gap[7] is still applicable to the beam with LR structures. The two resonant modes at T_1 and T_3 show that vertical vibration is the key factor for gap formation. As for the point T_2 [Fig. 4(b)], the vibration is also localized in the oscillators but it vibrates like a teetertotter due to the moment of inertia of the Cu ring. The two reso-

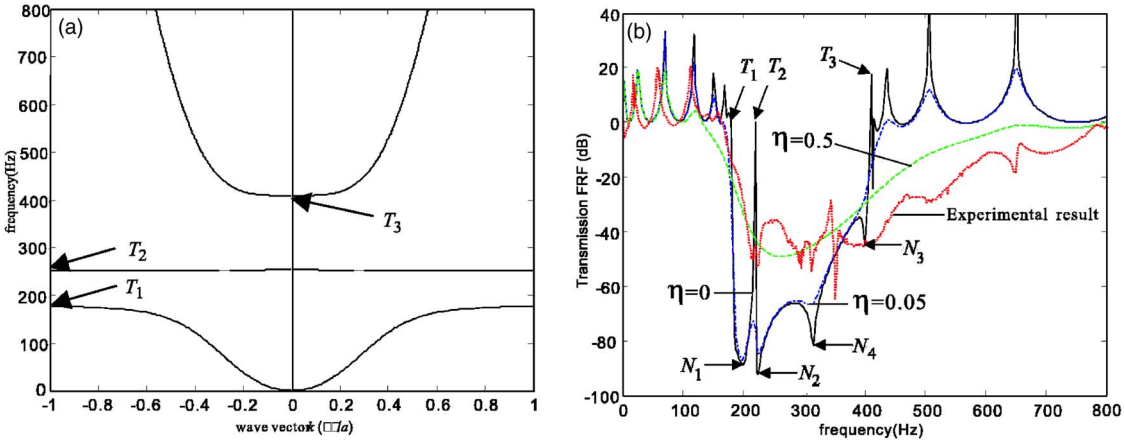

FIG. 3. (Color online) (a) Band structure of the Euler-Bernoulli beam with 2DOF LR structures, with lattice $a=1.5\times10^{-1}$ m. (b) Calculated and measured transmission FRF corresponding to samples of nine cells. The continuous, dash-dotted, and dashed lines represent the FRF calculated by the FE method with the structural damping coefficient of rubber material $\eta=0$, 0.05, and 0.5, respectively. The dotted line represents the measured result.

nant modes at T_1 and T_2 describe the two DOF of the resonators. For the antiresonant modes of T_1, T_2, and T_3, the vibration in the beam can be transferred to the resonators as a function of the dynamic vibration absorbers. Therefore three transmission minima appear in the FRF labeled as N_1, N_2, and N_3. But we find an additional transmission minimum inside the stop band at 315 Hz, labeled N_4. The deformation of the first cell is shown in Fig. 4(d); a vertical vibration coupled with torsional deformation in resonator can be found. So the minimum in the FRF at point N_4 appears. But the effect of the coupled vibration mode is not strong; there is no resonant peak appearing in the FRF.

From Fig. 4(a), the displacement of the aluminum tube is assumed to be negligible in comparison to the vibration of the resonators. So substituting Eqs. (7) and (8) into Eq. (5), using $y(x_n,t)=0$, we can obtain the vertical resonant frequencies at T_1 as

$$f_1 = \frac{1}{2\pi}\sqrt{\frac{2k}{m}} = 177 \text{ Hz}. \tag{21}$$

Analogously, the deformation of resonators at T_2 corresponding to the flat band in Fig. 3(a) is dominant as shown in Fig. 4(b). Using Eq. (6) and $y(x_n,t)=0$, we can obtain the torsional resonant frequencies at T_2 as

$$f_2 = \frac{1}{2\pi}\sqrt{\frac{2kl^2}{J}} = 250 \text{ Hz}. \tag{22}$$

The frequency f_1 is in very good agreement with the FRF. But as for frequency f_2, the rubber ring generates shear deformation [see Fig. 4(b)]; the rubber shear stiffness is less than the radial stiffness. So the rotational resonant frequency at T_2 is lower than f_2.

In order to verify the results calculated with the TM and the FE method, an Euler-Bernoulli beam with nine LR oscillators as in the simulation model in Fig. 3(a) was fabricated and a vibration experiment was performed. The test sample and the experimental system are shown in Figs. 5(a) and 5(b), respectively. We chose the experimental scheme that had been adopted earlier;[3] a white-noise signal with bandwidth from 0 to 1000 Hz is input into the vibration shaker, which transmits vibrations to the left end of the beam through the accelerometer. Then flexural waves propagate through the beam. The acceleration at the right end of the beam is measured with an accelerometer.

The dotted line in Fig. 3(b) illustrates the measured transmission FRF for this beam with nine LR oscillators. The frequency range of strong attenuation in the measured transmission FRF curve is from 170 to 785 Hz. Comparing with the theoretical result [continuous line in Fig. 3(b)], one can see two obvious differences. As shown in Fig. 3(b), the gap width becomes wider than the theoretical gap width and the resonant peak at T_2 in the theoretical FRF does not appear in the experimental result. The difference is completely due to the effect of the rubber material damping.

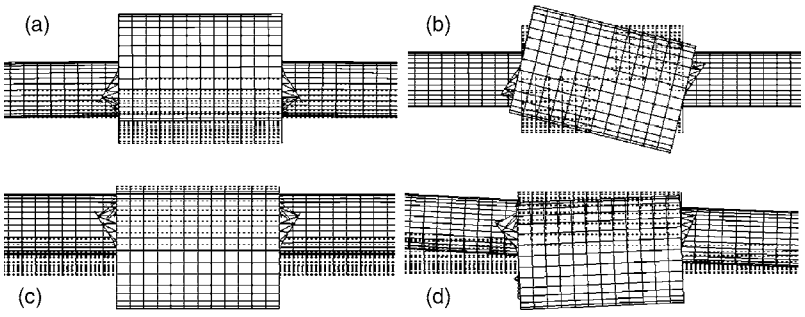

FIG. 4. The vibration deformation calculated by the FE method corresponding to corresponding to points (a) T_1, (b) T_2, (c) T_3, and (d) N_4 in Fig. 3, respectively. The dashed (solid) lines illustrate the primal (maximum) deformation, respectively.

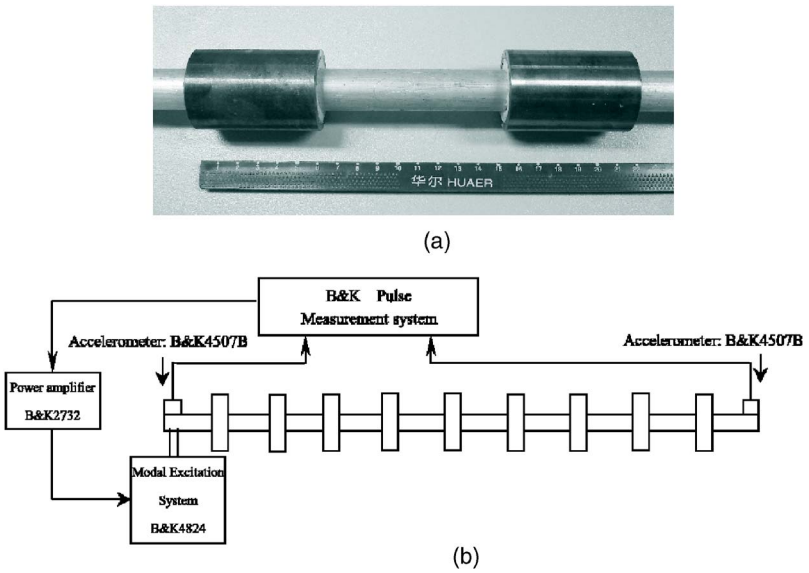

FIG. 5. (Color online) (a) Two periods of the test sample; (b) experimental instruments.

Now, we calculate the FRF with the effect of the structural damping coefficient of the rubber material. The dash-dotted and dashed lines in Fig. 3(b) represent the FRF with structural damping coefficients of the rubber material $\eta = 0.05$ and 0.5, respectively. From Fig. 3(b), we can draw the conclusion that the damping of the rubber will depress the resonant peak at T_2 even with a small damping coefficient. So the transmission maximum at T_2 on Fig. 3(b) cannot be measured in the experimental result. Also, the gap width will increase as the damping coefficient of rubber increases, but the maximum attenuation value in the gap decreases. So the transmission minima inside the stop band will vanish. When the damping coefficient of the rubber is $\eta = 0.5$, the theoretical and experimental results match well.

IV. CONCLUSIONS

In conclusion, low-frequency flexural wave band gaps in an Euler-Bernoulli beam with 2DOF LR structures are studied theoretically and experimentally. The dispersive relation was provided effectively by TM theory. A more physical understanding of the LR modes is investigated by a vibrational mode calculation using the FE method. Also the effect of the material damping in rubber was considered in the calculation. Finally an experimental system was designed to verify all the theoretical results. The measured result provides an attenuation of over 20 dB in the frequency range of the band gaps, which matches perfectly with the theoretical prediction. The gaps investigated in this paper provide a method for the flexural vibration control of beams.

ACKNOWLEDGMENT

This work was funded by the State Key Development Program for Basic Research of China (Grant No. 51307).

*Corresponding author. Email address: dianlongyu@nudt.edu.cn

[1] Z. Liu, X. Zhang, Y. Mao, Y. Y. Zhu, Z. Yang, C. T. Chan, and Ping Sheng, Science **289**, 1734 (2000).
[2] J. Wen, G. Wang, D. Yu, H. Zhao, and Y. Liu, J. Appl. Phys. **97**, 114907 (2005).
[3] C. E. Bradley, J. Acoust. Soc. Am. **96**, 1844 (1994).
[4] C. E. Bradley, J. Acoust. Soc. Am. **96**, 1854 (1994).
[5] W. M. Robertson, J. Ash, and J. M. McGaugh, Am. J. Phys. **70**, 680 (2002).
[6] G. Wang, J. Wen, and X. Wen, Phys. Rev. B **71**, 104302 (2005).
[7] G. Wang, X. Wen, J. Wen, L. Shao, and Y. Liu, Phys. Rev. Lett. **93**, 154302 (2004).
[8] Z. Liu, C. T. Chan, and P. Sheng, Phys. Rev. B **71**, 014103 (2005).
[9] Z. Liu, C. T. Chan, P. Sheng, A. L. Goertzen, and J. H. Page, Phys. Rev. B **62**, 2446 (2000).
[10] Z. Liu, C. T. Chan, and Ping Sheng, Phys. Rev. B **65**, 165116 (2002).
[11] C. Goffaux, J. Sánchez-Dehesa, A. L. Yeyati, P. Lambin, A. Khelif, J. O. Vasseur, and B. Djafari-Rouhani, Phys. Rev. Lett. **88**, 225502 (2002).
[12] C. Goffaux and J. Sánchez-Dehesa, Phys. Rev. B **67**, 144301 (2003).
[13] M. Hirsekorn, Appl. Phys. Lett. **84**, 3364 (2004).
[14] H. Qiao, Int. J. Mech. Sci. **44**, 725 (2002).
[15] J. J. Wu and A. R. Whittaker, J. Sound Vib. **227**, 361 (1999).
[16] J. S. Jensen, J. Sound Vib. **266**, 1053 (2003).
[17] S. Timoshenko, D. H. Young, and W. Weaver, Jr., *Vibration Problems in Engineering* (Wiley, New York, 1974).
[18] C. Kittle, *Introduction to Solid State Physics* (Wiley, New York, 1986).
[19] C. S. Zhao, Chin. Mech. Eng. **15**, 962 (2004) (in Chinese).